Int. J. Electrochem. Sci., 12 **(2017)** 3635 – 3651, doi: 10.20964/2017.05.52

International Journal of
ELECTROCHEMICAL
SCIENCE
www.electrochemsci.org

Influence of Pulse Operational Parameters on Electrodeposition, Morphology and Microstructure of Ni/nanodiamond Composite Coatings

M. Sajjadnejad[1,*], *H. Omidvar*[1,**], *M. Javanbakht* [2]

[1] Department of Mining and Metallurgical Engineering, Amirkabir University of Technology (Tehran Polytechnic), Tehran, Iran.
[2] Department of Chemistry, Amirkabir University of Technology (Tehran Polytechnic), Tehran, Iran.
[*]E-mail: m.sajjadnejad@yahoo.com
[**]E-mail: omidvar@aut.ac.ir

Received: 17 November 2016 / *Accepted:* 12 March 2017 / *Published:* 12 April 2017

Nickel and Nickel-nanodiamond coatings have been successfully electrodeposited on copper substrates by the pulse plating method. The variables investigated within this work include the current density, pulse frequency, bath temperature, duty cycle and nanodiamond concentration of the bath. Pure nickel coatings possess a preferred orientation along (111) crystal plane, however incorporation of the nanodiamond particulates in the platings increases the relative peak intensity corresponding to (200) crystal plane. It was found that presence of nanoparticles on the cathode surface leads to the formation of large nickel grains with [100] preferred orientation and small grains with [111] preferred orientation. X-ray diffraction studies demonstrated that incorporation of nanodiamond particulates to the nickel matrix causes negative lattice distortions in the nickel matrix. Presence of the nanodiamond particulates slightly decreases the current efficiency and deposition rate. Incorporation rate of nanodiamond particulates increases with decreasing current density and increasing pulse frequency. Maximum incorporation rate of 2.24 Vol.% was achieved at the duty cycle of 25%.

Keywords: Electrodeposition; Nanocomposite; Nanodiamond; Nickel; Microstructure; Morphology.

1. INTRODUCTION

Nickel possesses outstanding plating properties and is extensively used for coatings, both for decorative and engineering applications. In many cases, a finish coat such as chromium is used to change the appearance and hardness of Nickel coat. From a health standpoint, hexavalent chromium which is used in chrome plating contains a variety of carcinogenic compounds. Hence, those who partake in the chrome plating industry must act according to strict rules set forth by EPA

(Environmental Protection Agency). Besides, many developed countries are planning to reduce the use of nickel, too [1].

One strategy to reduce the use of chromium and nickel and enhance the corrosion and wear performance of nickel plates is to design novel nickel based composites. Enhancement of corrosion and wear resistance of nickel alloys by the incorporation of a variety of nanoparticles has been reported [2]. Among these nanoparticles, diamond is of special importance due to its unsurpassed hardness (table 1). Also, it has the highest thermal conductivity of any bulk material.

Table 1. Comparison of the hardness values of various filling materials on knoop scale (KH)[41].

Material	Hardness (Knoop)
SiC	2500
TiO_2	713
Al_2O_3	2000
WC	1730
Si_3N_4	1934
SiO_2	700
B_4C	2750
ZrO_2	1160
TiC	2470
Diamond	7000
Nanodiamond	>7000

These properties make diamond an excellent material for polishing, grinding and cutting tools and a variety of other extreme uses. Diamond can be used to wear away any other material. Industrial applications of diamond include diamond tipped saws, drill bits and grinding wheels. In addition, wear resistant parts are manufactured by coating substrate metals with a thin layer of diamond.

The synergy of the hard, corrosion and wear resistant nickel metal and the unique properties of diamond may provide several benefits such as:

- Improved wear resistance
- Enhanced thermal transfer
- Enhanced corrosion resistance
- No use of chrome

With the increasing availability of diamond micro and nanoparticles Ni-diamond composites have been investigated widely. Nanodiamond (ND) particulates used as filler material are produced by the detonation process. This process is capable of producing ND particulates with prices as low as 1000$/kg. Hence, adding ND to the plating bath has a negligible effect on the final cost of nickel deposit. Both electrodeposition [3-8] and electroless coating [9-11] methods have been used to

synthesis Ni-diamond composites. Electroless deposition method is usually slower and is unable to produce thick plates of metal [12, 13].

Electrodeposition is a simple, low cost process in which deposition rate and thickness of coating can be varied over a wide range. However, in conventional direct current electrodeposition as the process continues, a layer of negatively charged species covers the cathode surface. This layer obstructs the charged particles from reaching the deposit-electrolyte interface. Pulse electrodeposition is a modification in electrodeposition process. In pulse electrodeposition, the current is periodically turned on and off and the negatively charged layer discharges somewhat. This favors faster passage of the charged particles through the layer and increases the content of micro and nano sized reinforcement [14]. In pulse current electrodeposition, the duty cycle is defined as the percentage of total on-time of a cycle [14]:

$$\text{Duty cycle}(\gamma) = \frac{T_{ON}}{T_{ON}+T_{OFF}} = T_{ON}f \quad (1)$$

In this equation f represents pulse frequency [14]:

$$\text{Frequency} = \frac{1}{T_{on}+T_{off}} = \frac{1}{T} \quad (2)$$

The objective of this research work is investigating the effects of electroplating parameters on the volume percentage of diamond nanoparticles, deposition rate, current efficiency, morphology and microstructure of the deposit.

2. EXPERIMENTAL DETAILS

Table 2. Electrolyte composition and the electroplating parameters.

Variable	Range
$NiSO_4.6H_2O$	300 (g/l)
H_3BO_3	40 (g/l)
$NiCl_2.6H_2O$	40 (g/l)
SDS	0.3 (g/l)
Nanodiamond	10 (g/l)
Temperature	50,75 (^{0}C)
Peak current density	1,4,7,10 (A/dm^2)
Pulse frequency	1,10,50,100 (Hz)
Duty cycle	10,25,50,75 (%)
pH	4
Stirring rate	250 (rpm)

Nickel and nickel-nanodiamond (Ni-ND) coatings were electrodeposited on copper substrate in a glass cell .Nickel sheets (purity>99%) were used as anode and copper sheets (purity>99%) were used as cathode. Ni and Ni-ND coatings were obtained under pulsed current conditions. Nickel anode

(70mm×20mm×1mm) was chosen significantly larger than copper cathode (10mm×20mm×1mm) to avoid anodic polarization.

The electrolyte composition and electroplating parameters are presented in table 2. Unless otherwise stated the electrodeposition of the coatings were conducted at C_{ND}=10 g/l and T=50 ^{o}C. In order to prepare bath solution, boric acid, $NiSO_4.6H_2O$, $NiCl_2.6H_2O$ and Sodium Dodecyl Sulfate (SDS) were dissolved in water. Magnetic stirring was applied for 1 hour to dissolve ingredients in water. Nanodiamond particles were provided from Penta chemicals and used without any treatment. According to the manufacturer nanoparticles had a diameter of 4-6 nm, a density of 3.3 $g.cm^{-3}$ and a specific surface area of 282 $m^2.g^{-1}$. After adding ND powder, the bath solution was stirred for 12 hours and then ultrasonicated for 30 minutes to assure uniform distribution of the nanoparticles in the bath and inhibit nanoparticles agglomeration.

The copper cathode was polished, ultrasonicated in acetone, dipped in HCl (15%) and washed in distilled water. The surface morphology of prepared electrodeposits were studied by a field emission scanning electron microscope (FE-SEM, XL-30, PHILIPS). Each specimen was weighed before and after the electroplating process. Weight measurement values are average of at least two measurements and were used for the calculation of current efficiency. TEM imaging was employed to investigate the size distribution of ND reinforcement. Sample preparation involved ultrasonic dispersion of powder in ethanol for 30 min and nanoparticles drying on a copper grid that is coated with a thin layer of carbon. The microstructures of the composite coatings were studied employing X-ray diffraction (XRD). The thickness of the electrodeposits was measured using X-ray fluorescence spectroscopy (XRF).The thickness values are average of five measurements. Glow discharge optical emission spectroscopy (GDOES) was used to investigate composition changes along the coatings thickness and determine the weight and volume fraction of the diamond. Reported incorporation rates are average of two measurements.

3. RESULTS AND DISCUSSION

3.1 Characterization of ND powder

XRD was employed to study microstructure of ND powder as well as Ni and Ni-ND coatings structures. Fig. 1a presents the XRD pattern of the ND powder. The characteristic peaks of diamond can be seen at $2\theta=44^0$ corresponding to (111) crystal plane and a smaller peak at $2\theta=75^0$ corresponding to (200) crystal plane. The diffraction peak width corresponding to the powder is very wide, indicating that ND powder possesses ultrafine crystallites. Average size of 4.26 nm was calculated for powder grains using full width of (111) peak at half maximum (FWHM). However, there are several sources of peak broadening. Crystal lattice distortion, structural mistakes and concentration gradients contribute to peak broadening. Also, instrumental contributions such as not perfectly monochromatic radiation result in peak broadening. In order to find the accurate size of the nanoparticles TEM imaging was employed (Fig. 1b). Nanoparticles with different sizes from 5 to10 nm were observed.

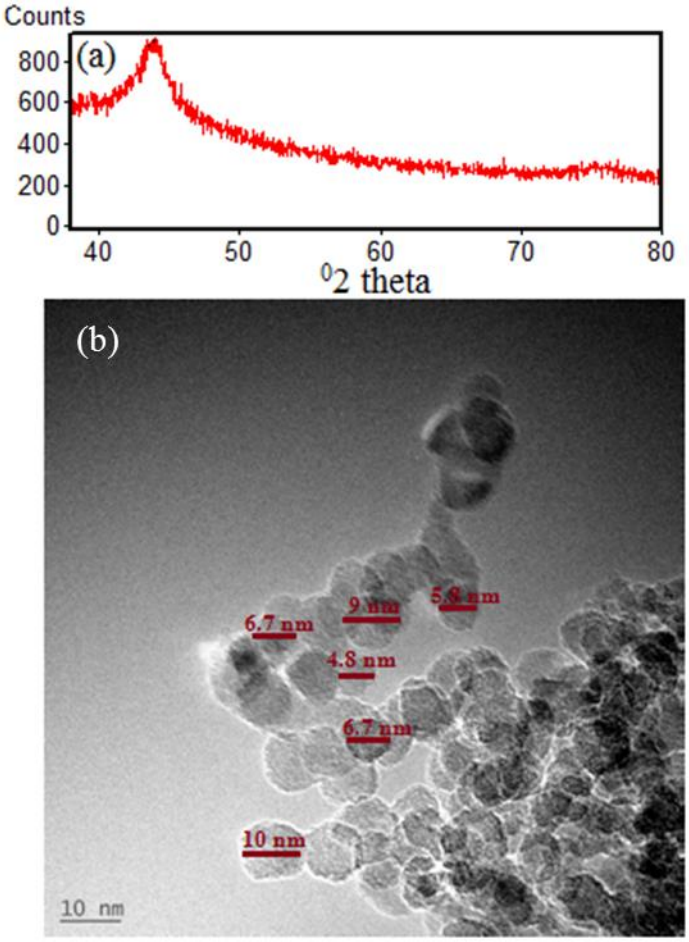

Figure 1. (a) XRD pattern and (b) TEM image of ND powder.

3.2 Structural analysis of Ni-ND

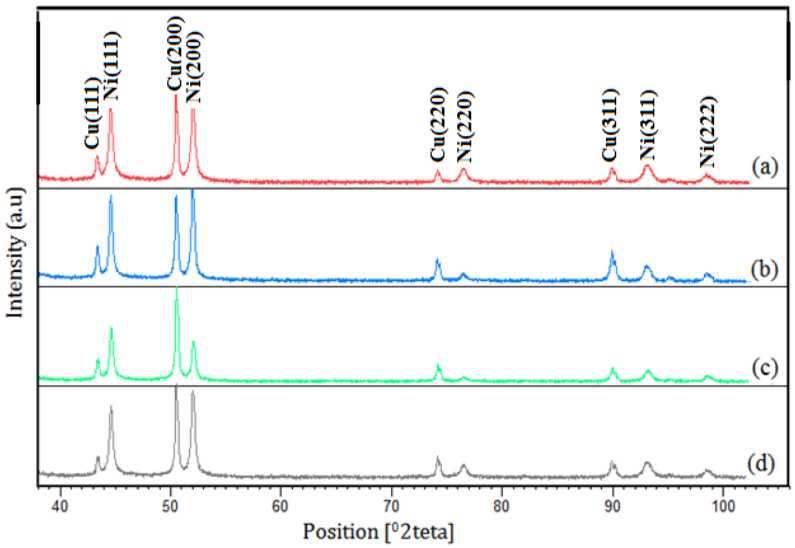

Figure 2. XRD patterns of Ni-ND electrodeposits at (a, b) γ=10, 75 %, I_p= 4 A/dm^2, f=10 Hz (c, d) f=1, 100 Hz, I_p= 4 A/dm^2, γ=50%.

For Ni-ND electrodeposits, the diffraction angle of (111) lattice planes of nickel is very close to that of the diamond (111) plane resulting in a peak overlap. Hence, ND diffraction peaks could not be detected in XRD spectra corresponding to the Ni-ND composites (Fig. 2). All of the Ni and Ni-ND electrodeposits have a single phase of nickel matrix with face centered cubic (FCC) crystal structure. In order to quantify the influence of the electroplating parameters on the texture and preferred orientation of Ni-ND composites, the texture coefficients (TC) were calculated, as defined in eq. (3) [15]:

$$TC(hkl) = \frac{\frac{I(hkl)}{I_0(hkl)}}{\frac{1}{n}\sum\frac{I(hkl)}{I_0(hkl)}} \quad (3)$$

Where I(hkl) and I_0(hkl) are the measured and standard intensity (JCPDS 4-0850) of the (hkl) reflection, respectively. n is the number of reflections used in the calculation (5 reflections were used: (111), (200), (220), (311), (222)).

Table 3. Texture coefficient of (111) and (200) crystal planes, crystallite size of the deposits and lattice distortions of nickel matrix.

Coating	i (A/dm^2)	f (Hz)	$\gamma(\%)$	$TC_{(111)}$	$TC_{(200)}$	Crystallite Size (nm)	Distortion%
Ni-ND	1	10	50	1.47	2.16	41	-0.29
Ni-ND	4	10	50	1.35	2.64	41	-0.22
Ni-ND	10	10	50	0.89	3.42	47	--0.20
Ni-ND	4	10	10	1.18	2.62	37	-0.21
Ni-ND	4	10	75	0.16	3.31	48	-0.16
Ni-ND	4	1	50	1.68	2.12	32	-0.3
Ni-ND	4	100	50	0.96	3.36	42	-0.18
Ni	4	10	50	1.79	1.91	46	-0.13

Table 3 presents the data obtained from X-ray diffraction tests.TC numbers greater than1 evidence the existence of a preferred orientation. Pure nickel coatings possess a preferred orientation along (111) crystal plane, however presence of ND in the platings increases the relative intensity corresponding to (200) crystal plane. The peak intensity corresponding to the (200) crystal plane increased with increasing pulse frequency. The same observations were made when duty cycle was increased. At γ=75%, a $TC_{(200)}$ of 3.16 and $TC_{(111)}$ of 0.16 were observed which means strong (200) preferred orientation. Application of higher current density led to orientation along the (200) crystal plane, too. According to Chen et al. [16] at low growth rates, Ni incline to crystallization in (111) crystal plane due to high atom density ($\frac{1}{2R^2\sqrt{3}}$, R is nickel atoms radius) and consequently lower surface energy. In case of pulse plating process, a higher growth rate is obtained, hence some of the Ni^{2+} ions were not capable of crystallization in (111) crystal plane, consequently they rest on (200)

crystal plane. A high duty cycle means a short off-time and provides less time to the fresh Ni atoms to transfer to a stable position during the off time. Hence, more Ni atoms crystalize in (200) crystal plane.

Another explanation for microstructural evolution of nickel electrodeposits is suggested by Amblard et al. [17, 18]. Amblard believes that "inhibition effect" exerted by the species such as H^+ and OH^- plays an essential role in the electrocrystallization of nickel. Ni has a high surface energy and readily absorbs any kind of chemisorbable species. These absorbed species occupy active surface areas of the cathode and exert inhibition. For example, at very low current densities ($i<1$ A/dm^2) the growing surface of the deposit is covered b the H^+ ions and all the growth directions are inhibited except [110]. According to them [100] is the free mode of growth for nickel electrodeposits and they attribute the [111] direction to sever inhibition by the $Ni(OH)_2$. Hence, we may conclude that incorporation of the nanodiamond particles provides fresh active surface area for nickel deposition and consequently enhances free mode of growth ([100] direction).

The crystallite size of the deposits was determined using the Scherrer equation [19]:

$$D = \frac{0.9\lambda}{\beta Cos\Theta} \quad (4)$$

In this equation, D shows the crystallite size value, β represents the peak width at half-maximum intensity, λ is equal to the wavelength of the incident radiation (0.15418 nm) and θ represents the bragg angle.

The variations in crystallite size of the composites electrodeposited under different conditions, may be attributed different nucleation rate and overpotential. The rate of nuclei formation and overpotential are related [20]:

$$\text{nucleation rate} = k_1 \exp\left(\frac{k_2}{\eta^2}\right) \quad (5)$$

Where k_1, k_2 are constants and η is deposition overpotential. Microstructure refinement was expected with the application of the higher current densities (table 3). High current density leads to increased overpotential and consequently enhances the nucleation rate. Coarse microstructure at high duty cycle and pulse frequency may be attributed to formation of large grains with [100] orientation [21].

Lattice distortions of Ni–ND coatings were estimated using basic reflections of their crystal planes. The results evidenced that the Ni-ND lattice constants depend on f, i and γ as presented in table 3. The Lattice constant for a face-centered cubic (fcc) system can be determined using the following equation [22]:

$$a^2 = \left(\frac{\lambda^2}{4(\sin\theta)^2}\right)(h^2 + k^2 + l^2) \quad (6)$$

The deviation in the lattice constant was calculated as follows [22]:

$$Distortion\% = 100\left(\frac{a_0 - a_1}{a_0}\right) \quad (7)$$

Where a_0 is the lattice constant of nickel in absence of stress and a_1 is the lattice constant of the nickel matrix in Ni-ND coating. Incorporation of ND particulates to the nickel matrix causes negative lattice distortions in the nickel matrix. The same results are reported in previous studies on Ni-SiC and Ni-Al_2O_3[22, 23].

The reasons for negative lattice distortion in Ni-ND composite coatings can be explained by 3 types of stresses[24]:

(1) Stresses originating from differing lattice parameter (copper substrate and nickel metal).

(2) Thermal stresses caused by different thermal expansion coefficients at the nickel and copper interface.

(3) Intrinsic stress resulting from bath composition and plating conditions.

As it is seen in table 3, commonly the distortion values are very low. This is especially important because high lattice distortion may contribute to the peak broadening and result in high error values in crystallite size calculations.

3.3 Morphological studies

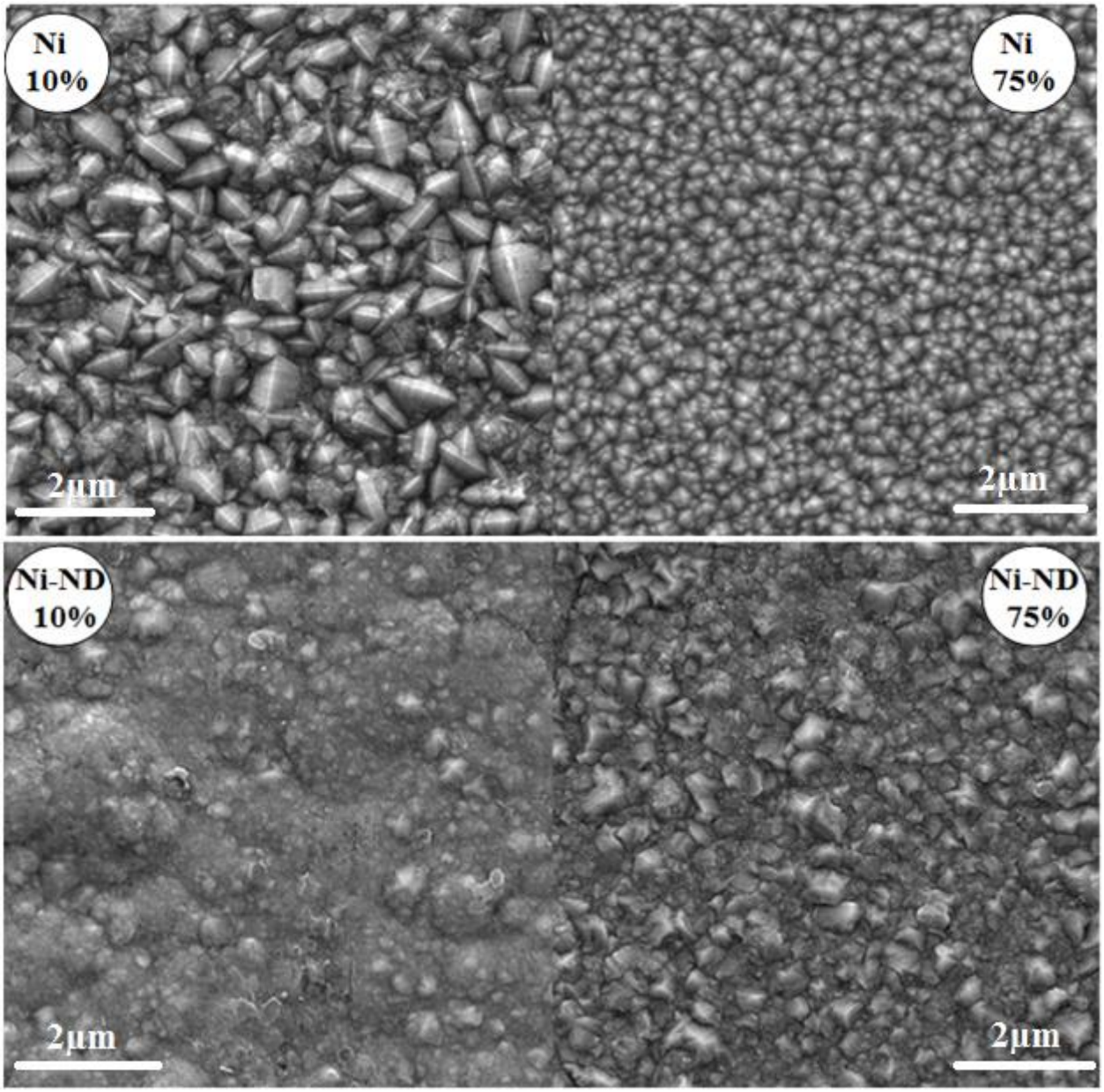

Figure 3. FE-SEM micrograph of Ni and Ni-ND deposits obtained at I_p= 4 A/dm^2 and □=10 Hz.

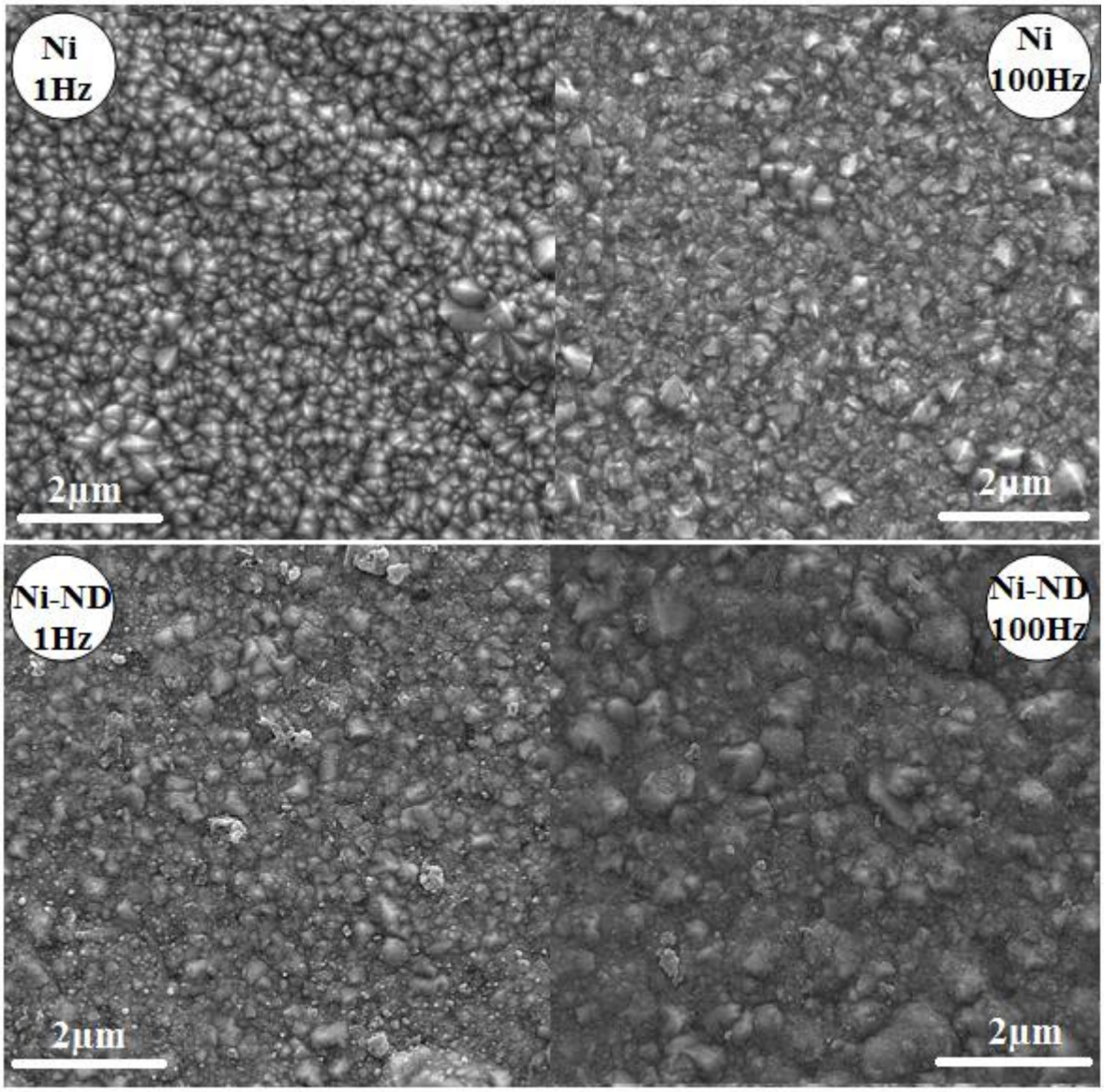

Figure 4. FE-SEM micrographs of Ni and Ni-ND deposits obtained at I_p= 4 A/dm^2, □=50 %.

It can be seen in Fig. 3a and b that pure nickel coatings possess a truncated pyramidal structure. This is a usual morphology for pure nickel electrodeposits with (111) preferred texture [25, 26]. The modifications in the surface morphologies is attributed to the modification from a preferred orientation to a random oriented electrodeposit [27]. The addition of ND particulates deteriorates the pyramidal structure.

In case of pure nickel coatings, coatings obtained under 75% duty cycle conditions consist of smaller grains. Duty cycle of 75% leads to an ion deficient area around the deposit due to differences in Ni^{2+} ions crystallization rate at the cathode surface and the diffusion rate of Ni^{2+} cations towards the cathode. Consequently the deposition overpotential and rate of nuclei formation increases and the size of grains becomes smaller.

Contrarily, for Ni-ND coatings some very large grains with irregular structure were observed at duty cycle of 75%. These grains have a [100] orientation [21]. Hence, in this case the variations in

grain orientation leads to changes in grain size. The Ni-ND coating obtained at duty cycle of 10% seems to be very compact and possess fewer gaps compared to other coatings. This may be attributed to very small on-time and extensive off-time. These conditions results in high Ni^{2+} concentration near the deposit-electrolyte interface and favors lateral growth [28].

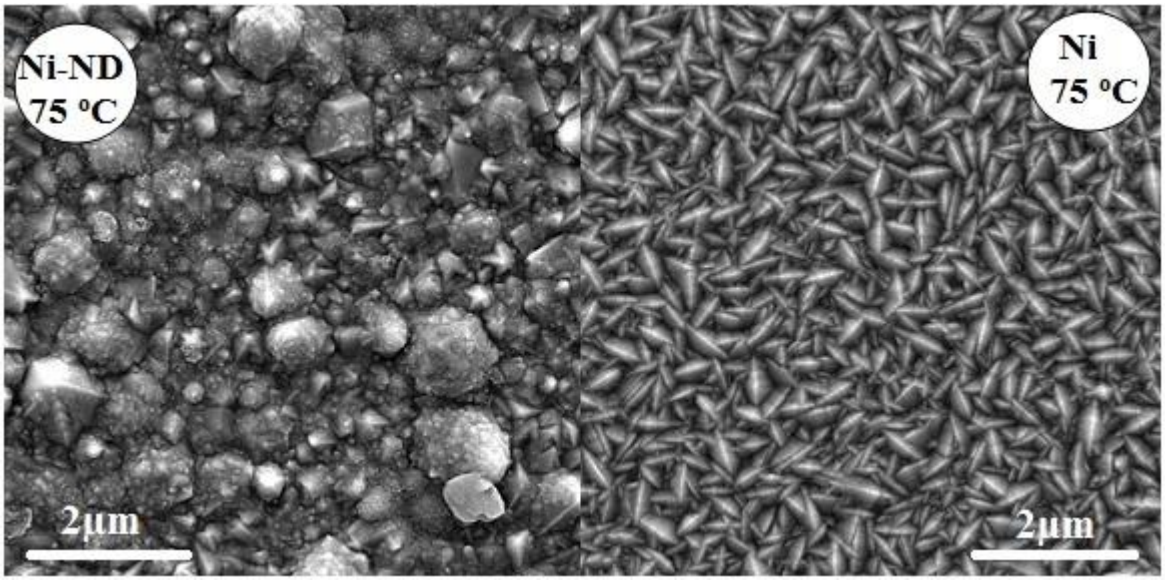

Figure 5. FE-SEM micrographs of Ni and Ni-ND deposits obtained at i_p= 4 A/dm^2, □=50 %, f=10Hz.

In pure nickel coatings obtained at f=1 Hz many grains with binary symmetry were observed which is typical of grains with [211] orientation (crystallization on (111), (311) and (222) crystal planes may lead to a dispersed [211] preferred orientation [21]). When applying high pulse frequencies a considerable change in the topography of the pure nickel and nickel-ND coatings was observed. For nickel electrodeposits obtained at f=100 Hz, grains grew with irregular sizes and geometrical shapes. Similar morphologies were observed for Ni-ND deposits both at 1 and 100 Hz. Again, large grains are result of electrocrystallization on (200) crystal plane and smaller ones probably are result of electrocrystallization on (111) crystal plane.

Two of the coatings were deposited at 75 ^{o}C (Fig.5).The cathodic overpotential is lower at high the bath temperatures. Hence, the grains of the coatings were larger at high bath temperatures [29]. However, it is noteworthy to remind that bath temperature has two contradictory influences [30]:

1. At higher temperatures the critical size of nucleus is larger which results in formation of fewer stable nucleus and consequently coarser grains.
2. The kinetic driving force is higher at high temperatures which enhances the nucleation rate and smaller grains.

If the size of critical clusters is very large, although according to Arrhenius equation the nucleation rate increases with increasing temperature, the thermodynamic barriers for nucleation is considerable and few of the active sites act as a critical nucleus. Hence, these conditions lead to coarse grains.

3.4 ND incorporation rate

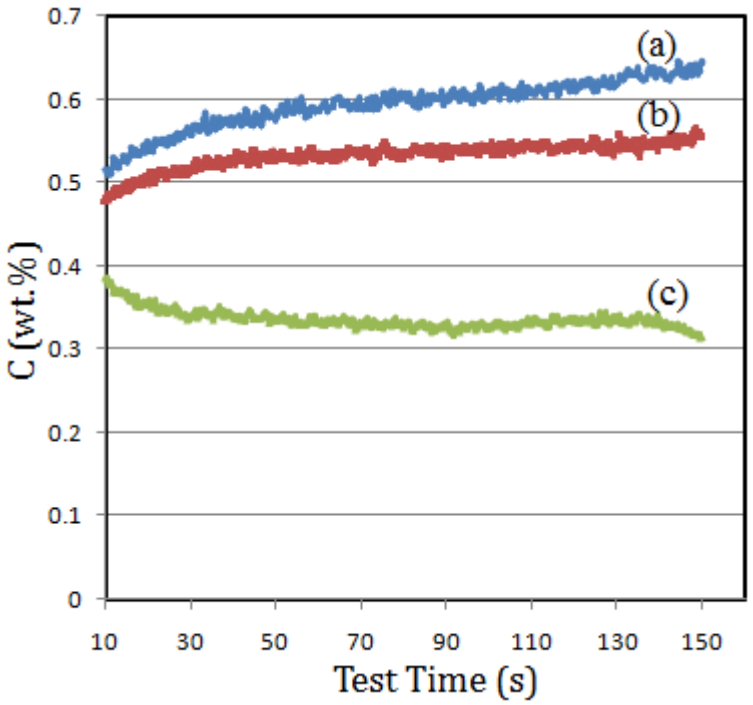

Figure 6. GDOES results on Ni-ND samples obtained at (a) i_p= 4 A/dm^2, □=10 %, f=10Hz (b) i_p= 10 A/dm^2, □=50 %, f=10Hz (c) i_p= 4 A/dm^2, □=75 %, f=1Hz.

GDOES profiles of Ni and Ni-ND coatings were recorded to evaluate the ND content of the coatings and study ND particles distribution in the depth of the deposits. Three representative results are depicted in Fig.6. The results confirm even distribution of ND particulates throughout the film. The volume fractions of ND particulates were calculated using the average weight fraction values obtained from two separate GDOES tests, on the same coating. The ND incorporation decreases with the changes in current density from 1 up to 10 A/dm^2 (Fig. 7a). These results evidence that diffusion of nickel ions from solution towards the cathode was faster than ND particles [31]. Hence, rapid electrodeposition of the nickel ions leads to a decrease in ND content of the composites.

Application of higher pulse frequencies results in higher overpotential and enhances the embedding particles in the nickel matrix [32]. Hence, it's not surprising that particle incorporation rate at 10, 50 and 100 Hz is considerably higher than that of 1 Hz (Fig.7b). The incorporation rate of ND particles increases with the duty cycle and reaches a maximum at γ=25% (Fig.7c).This observation can be associated with the fact that at duty cycles of 10% by the short on-time and long off-time, loosely adsorbed ND particulates may be detached by solution flow [33]. By increasing γ to 25% this problem is avoided and maximum ND incorporation is achieved. As γ increases to 50% or 75% the amount of embedded ND particulates decreased due to higher average current density.

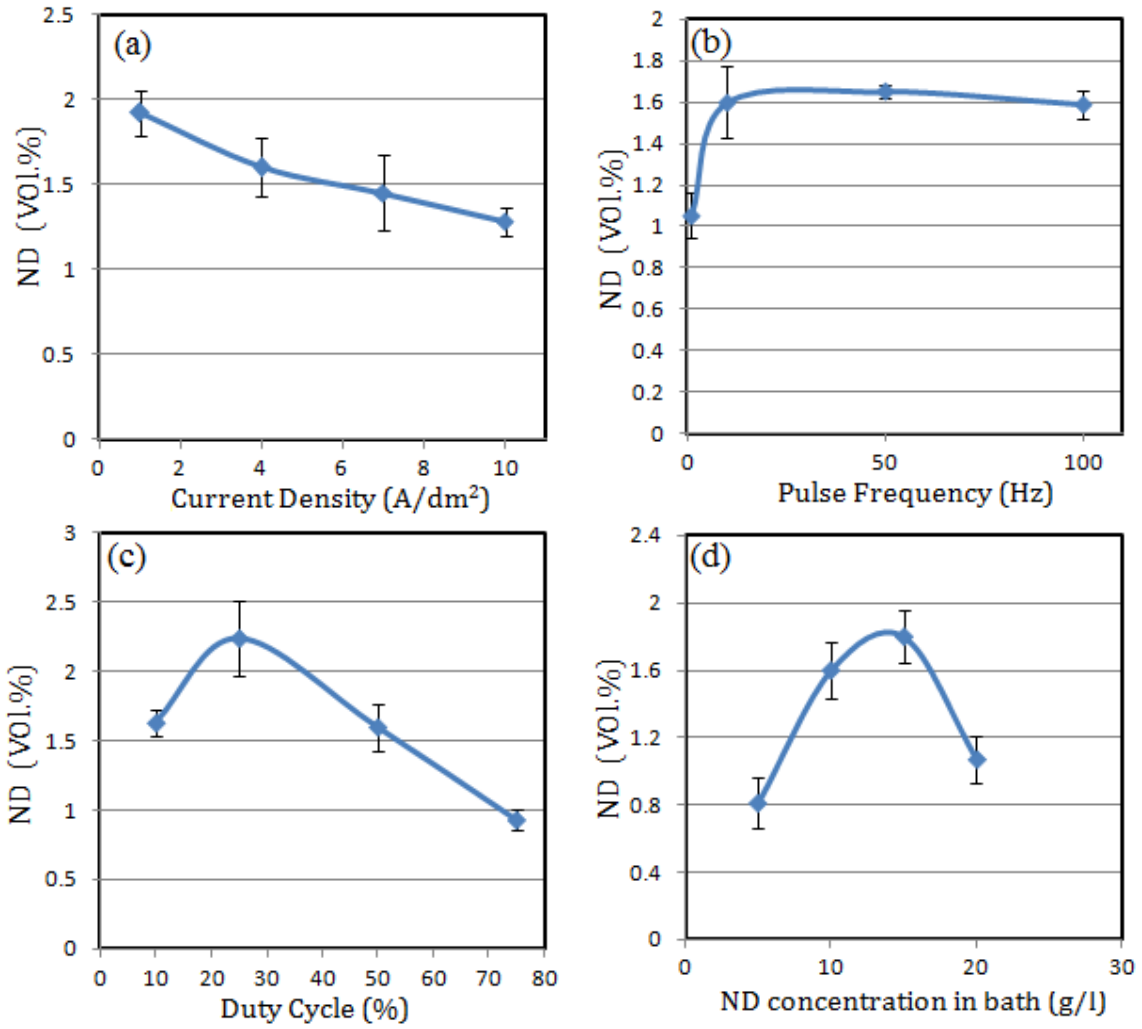

Figure 7. ND content of the Ni-ND composite as a function of electroplating parameters (a) γ=50 %, f=10 Hz (b) γ=50 %, i_p= 4 A/dm^2 (c) f=10 Hz, i_p= 4 A/dm^2 (d) γ=50 %, f=10 Hz, i_p= 4 A/dm^2.

The ND content of the composites increases with ND concentration of the bath (Fig. 7d). This is in agreement with the Gugliemi's model [34] for electrodeposition of the composite coatings. Decrease in incorporation rate of ND particles in composites obtained from solutions containing 20 g.L^{-1} ND, could be attributed to the agglomeration of the particles [35].

3.5 Deposition rate

One of the aims of this research work was to investigate the dependence of the deposition rate of the composite on plating parameters and find the optimum conditions for the electrodeposition of pure nickel and Ni-ND composites. Effects of different conditions on deposition rate are shown in figures 8. It is reported that presence of nanoparticles in the electrolyte increases the deposition rate [36].

However, in this research work it was observed that deposition rates of Ni and Ni-ND coatings were almost equal or sometimes deposition rate of the Ni-ND was slightly lower. The deposition rate

of the Ni-ND coatings increases linearly with increasing current density from 1 to 7 A/dm^2 .It can be predicted form Fig. 8a that beyond 10 A/dm^{2}deposition rate of Ni-ND coating remains almost constant. This can be explained by the polarization at the cathode surface with increasing current density and under these conditions the rate of deposition is determined by the rate of transport of the Ni^{2+}ions to the cathode surface [37].

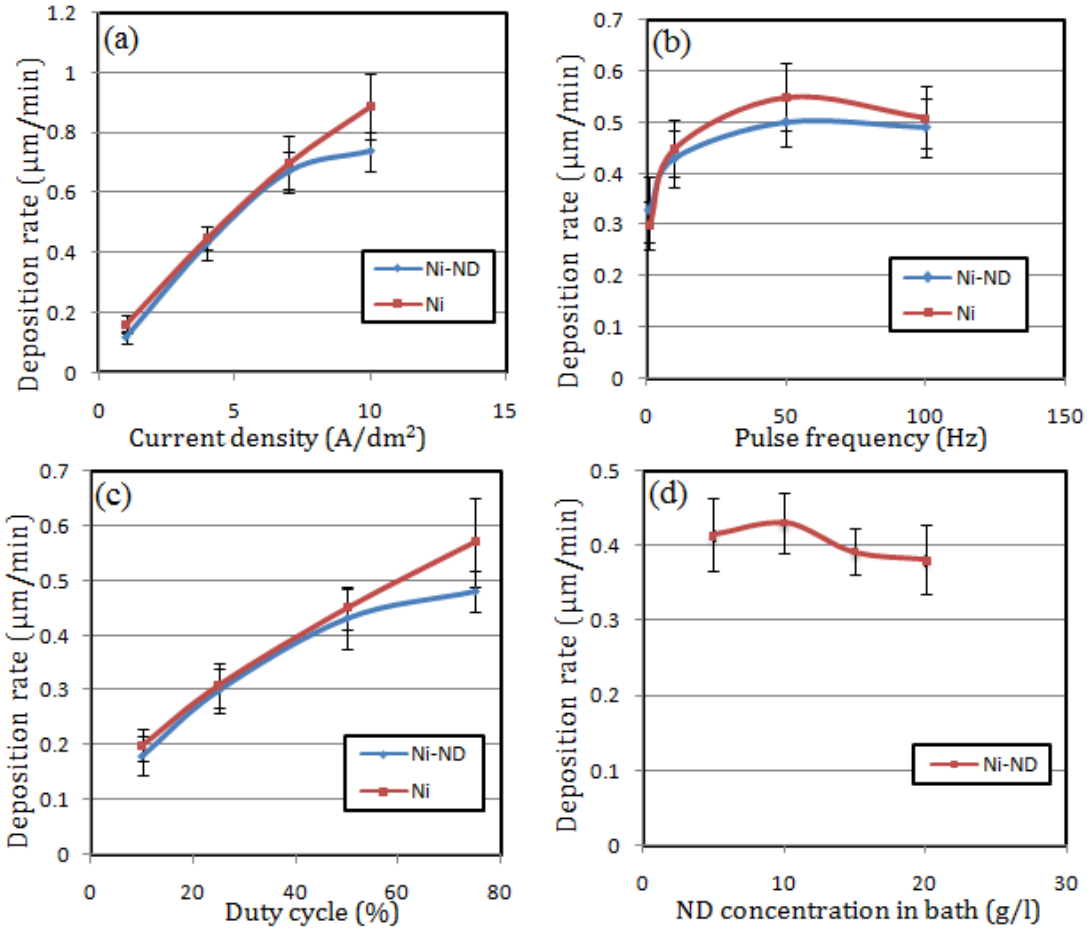

Figure 8. Deposition rate of the Ni and Ni-ND electrodeposits as a function of electroplating parameters at (a) γ=50 %, f=10 Hz (b) γ=50 %, i_p= 4 A/dm^2 (c) i_p= 4 A/dm^2, f=10 Hz (d) γ=50 %, i_p= 4 A/dm^2, f=10 Hz.

High pulse frequencies result in high deposition rates (Fig. 8b). At low pulse frequencies an ion deficient area forms around the cathode during the extensive off-time. Hence, deposition rate is lower at low pulse frequencies. The effect of duty cycle on deposition rate was similar to the effect of current density (Fig. 8c). Again, one may say that at high duty cycle with the extensive on-time and short off-time, polarization occurs at the cathode surface lowering deposition rate. According to the results ND content of the solution has a negligible influence on the deposition rate of Ni-ND composite coating (Fig. 8d).

According to the literature the deposition rate of the nickel electrodeposits may be increased by rising the electrolyte flow and optimizing the distance between the substrate and nickel anode [38]. Pollet et al. [39] reported that ultrasonic-assisted electrodeposition has a higher deposition rate in

comparison to conventional electrodeposition due to reduced polarization. The choice between pulse reverse and pulsed current electrodeposition techniques greatly favors the latter. According to Chandrasekar et al.[14] pulse reverse electrodeposition has a low net rate of deposition and deposition rate decreases with increasing the magnitude and duration of the reverse pulse.

3.6 Current efficiency

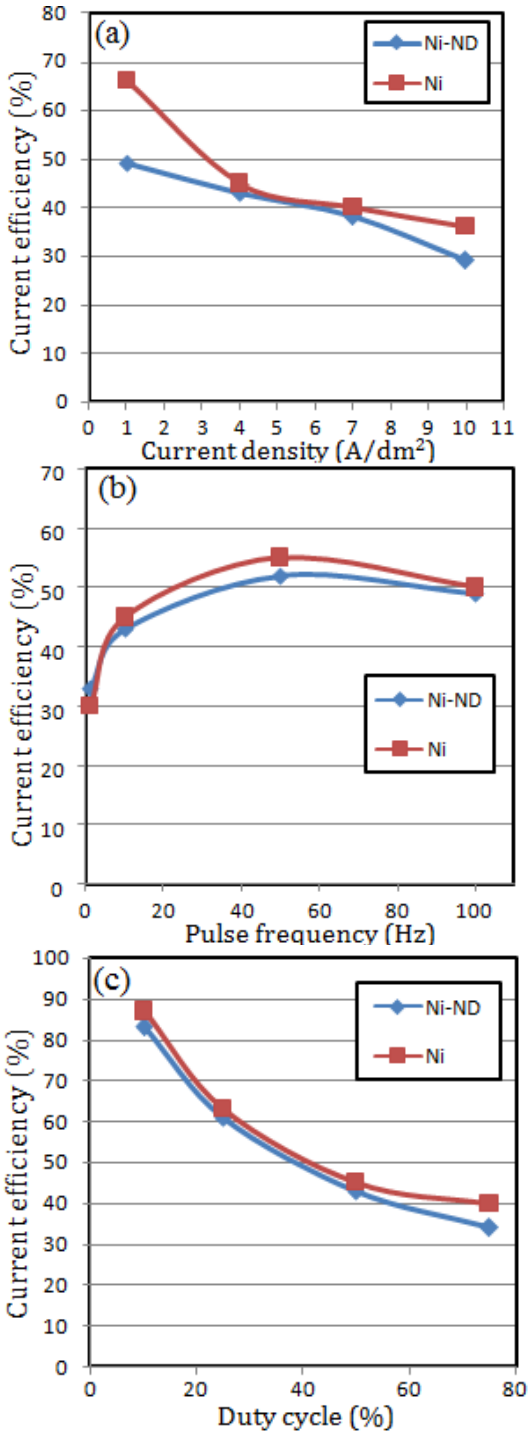

Figure 9. Current efficiency as a function of electroplating parameters (a) γ=50 %, f=10 Hz (b) γ=50 %, i_p= 4 A/dm^2 (c) i_p= 4 A/dm^2, f=10 Hz.

Current efficiency of the pulse current electrodeposition process can be calculated using the following equation:

$$\eta(\%) = \frac{m}{\frac{MI_a t}{ZF}} \quad (8)$$

Where z is valence, m is mass of deposited nickel, M is molar mass of nickel (58.7 gr/mol), I_a is average current and t is the electrodeposition time. Average current is defined as:

$$I_a = I_p \gamma = \frac{I_p T_{on}}{T_{on}+T_{off}} \quad (9)$$

Where I_p is peak current. Fig. 9a presents the effects of peak current density on η. It was observde that η decreases with increasing applied current density. The effect of i_p in reducing η has two reasons:

i. At higher current densities, the high rate of Ni^{2+} consumption results in lowering of Ni^{2+} concentration on the cathode surface and lowers current efficiency.

ii. At higher current densities, the decomposition of water and hydrogen evolution increases current loss.

Similarly at low pulse frequency and high duty cycle, low Ni^{2+} concentration at the cathode surface leads to low current efficiency.

Current efficiency slightly decreases in presence of ND particulates. This may be attributed to [36]:

i. H^+ ion film forms around each ND particulate immersed in the electrolyte which leads to facilitated transfer of the hydrogen ions towards the cathode and their faster reduction. These results are in agreement with observations made by Dolati et al.[40]. They believe that nanoparticles play a catalytic role in conversion of H^+ to H_{ads}.

ii. Attachment of ND particulates to the cathode surface perturbs nickel growth. This reduces the current efficiency of the electrodeposition process.

4. CONCLUSIONS

Pure nickel and Ni-ND coatings with maximum incorporation rate of 2.24 vol.% were prepared. Incorporation rate of ND increases with increasing pulse frequency up to 10 Hz and duty cycle up to 25%. Almost always presence of nanodiamond particles leads to formation of a mix microstructure of fine and coarse grains. X-ray diffraction studies revealed that application of high current density and duty cycle leads to orientation along the (200) crystal plane. Raising temperature encouraged formation of coatings with coarse grains. Deposition rate of Ni and Ni-ND coatings increased with pulse frequency, current density and duty cycle. Maximum current efficiency was achieved at duty cycle of 10%.

ACKNOWLEDGEMENTS

The authors gratefully acknowledge Mr. K. Langoori for his helpful comments and also National Iranian Gas Company (NIGC) for their financial support.

References

1. G. Burkat, T. Fujimura, V.Y. Dolmatov, E. Orlova and M. Veretennikova, *Diamond relat. mater.*, 14 (2005) 1761-1764.
2. H. Omidvar, M. Sajjadnejad, G. Stremsdoerfer, Y. Meas and A. Mozafari, *Mater. Manuf. Process.*, 31 (2015) 24-30.
3. E.C. Lee and J.W. Choi, *Surf. Coat. Technol*., 148 (2001) 234-240.
4. H. Abi-Akar, C. Riley and G. Maybee, *Chem. Mater.*, 8 (1996) 2601-2610.
5. K. Ramanathan, V. Periasamy, M. Pushpavanam and U. Natarajan, *ACMSSE*., 1 (2009) 232-236.
6. G.K. Burkat, T. Fujimura, V.Y. Dolmatov, E.A. Orlova and M.V. Veretennikova, *Diamond Relat. Mater.*, 14 (2005) 1761-1764.
7. W.H. Lee, S.C. Tang and K.C. Chung, *Surf. Coat. Technol*., 120–121 (1999) 607-611.
8. L. Guoqin, C. Guanxiong and H. Bin, *Surf. Technol.*, 3 (1991) 005.
9. C.C. Hung, C.C. Lin and H.C. Shih, *Diamond Relat. Mater.*, 17 (2008) 853-859.
10. V. Reddy, B. Ramamoorthy and P.K. Nair, *Wear*, 239 (2000) 111-116.
11. M. Pushpavanam, H. Manikandan and K. Ramanathan, *Surf. Coat. Technol.*, 201 (2007) 6372-6379.
12. F.H. Assaf, A.M.A Elsheidy, M.M. Abu Krisha and A.A. Eissa, *Int. J. Electrochem. Sci*., 7 (2015) 5465-5478.
13. T.H. Tsai, S. Thiagarajan and S.M. Chen, *Int. J. Electrochem. Sci.*, 6 (2011) 3878-3889.
14. M. Chandrasekar and M. Pushpavanam, *Electrochim. Acta*, 53 (2008) 3313-3322.
15. M. Karbasi, N. Yazdian and A. Vahidian, *Surf. Coat. Technol*., 207 (2012) 587-593.
16. L. Chen, L. Wang, Z. Zeng and T. Xu, *Surf. Coat. Technol.*, 201 (2006) 599-605.
17. J. Amblard, I. Epelboin, M. Froment and G. Maurin, *J. Appl. Electrochem*., 9 (1979) 233-242.
18. C. Kollia, N. Spyrellis, J. Amblard, M. Froment and G. Maurin, *J. Appl. Electrochem.*, 20 (1990) 1025-1032.
19. H. Sohrabi, S. Tabaian, H. Omidvar, M. Sajjadnejad and A. Mozafari, *Synth. Reac. Inorg.* M., 46 (2015) 414-422.
20. H. Omidvar, M. Sajjadnejad, G. Stremsdoerfer, Y. Meas and A. Mozafari, *Anti Corros. Method.Mater.*, 62 (2015) 116-122.
21. I. Tudela, Y. Zhang, M. Pal, I. Kerr, T.J. Mason and A.J. Cobley, *Surf. Coat. Technol.*, 264 (2015) 49-59.
22. H. Gül, F. Kılıç, M. Uysal, S. Aslan, A. Alp and H. Akbulut, *Appl. Surf. Sci*., 258 (2012) 4260-4267.
23. H. Gül, M. Uysal, H. Akbulut and A. Alp, *Surf. Coat. Technol.*, 258 (2014) 1202-1211.
24. A. El-Sherik, J. Shirokoff and U. Erb, *J. Alloy. Compd.*, 389 (2005) 140-143.
25. S. Pathak, M. Guinard, M.G. Vernooij, B. Cousin, Z. Wang, J. Michler and L. Philippe, *Surf. Coat. Technol.*, 205 (2011) 3651-3657.
26. A. Godon, J. Creus, X. Feaugas, E. Conforto, L. Pichon, C. Armand and C. Savall, *Mater. Charact.*, 62 (2011) 164-173.
27. M. Srivastava, V.W. Grips and K. Rajam, *Appl. Surf. Sci.*, 253 (2007) 3814-3824.
28. T. Frade, V. Bouzon, A. Gomes and M. da Silva Pereira, *Surf. Coat. Technol.*, 204 (2010) 3592-3598.
29. A. Rashidi and A. Amadeh, *J. Mater. Sci. Technol.*, 26 (2010) 82-86.
30. J. Vazquez-Arenas, R. Cruz and L.H. Mendoza-Huizar, *Electrochim. Acta*, *5*2 (2006) 892-903.
31. M. Sajjadnejad, H. Omidvar, M. Javanbakht, R. Pooladi and A. Mozafari, *Trans. Inst. Met. Finish.*, 92 (2014) 227-232.
32. S. Spanou and E. Pavlatou, *J. Appl. Electrochem.*, 40 (2010) 1325-1336.
33. S. Lajevardi and T. Shahrabi, *Appl. Surf. Sci.*, 256 (2010) 6775-6781.
34. N. Guglielmi, *J. Electrochem. Soc.*, 119 (1972) 1009-1013.

35. M. Sajjadnejad, M. Ghorbani and A. Afshar, *Ceram. Int.*, 41 (2015) 217-224.
36. M. Salehi Doolabi, S. Sadrnezhaad, D. Salehi Doolabi and M. Asadirad, *Int. Heat Treat. Surf. Eng*., 6 (2012) 178-184.
37. M. Vaezi, S. Sadrnezhaad and L. Nikzad, *Colloid. Surface.* A., 315 (2008) 176-182.
38. M. Schlesinger and M. Paunovic, *Modern electroplating*, John Wiley & Sons, 2011.
39. B. Pollet, J. Lorimer, S. Phull, T. Mason, D. Walton, J. Hihn, V. Ligier and M. Wéry, *J. Appl. Electrochem.*, 29 (1999) 1359-1366.
40. A. Sohrabi, A. Dolati, M. Ghorbani, M.R. Barati and P. Stroeve, *J. Physic. Chem.*, C 116 (2012) 4105-4118.
41. F. James, F. Shackelford and W. Alexander, *Materials Science and Engineering Handbook*, CRC Press, LLC, 2001.